npj | quantum materials

Article

Published in partnership with Nanjing University

https://doi.org/10.1038/s41535-024-00632-8

Flat-band hybridization between *f* and *d* states near the Fermi energy of $SmCoIn_5$

David W. Tam [1] ✉, Nicola Colonna [1,2,3], Fatima Alarab [4], Vladimir N. Strocov [4], Dariusz Jakub Gawryluk [5], Ekaterina Pomjakushina [5] & Michel Kenzelmann [1] ✉

We present high-quality angle-resolved photoemission (ARPES) and density functional theory calculations (DFT+U) of $SmCoIn_5$. We find broad agreement with previously published studies of $LaCoIn_5$ and $CeCoIn_5$[1,2], confirming that the Sm 4*f* electrons are mostly localized. Nevertheless, our model is consistent with an additional delocalized Sm component, stemming from hybridization between the 4*f* electrons and the metallic bands at "hot spot" positions in the Brillouin zone. The dominant hot spot, called γ_Z, is similar to a source of delocalized *f* states found in previous experimental and theoretical studies of $CeCoIn_5$[1,3]. In this work, we identify and focus on the role of the Co *d* states in exploring the relationship between heavy quasiparticles and the magnetic interactions in $SmCoIn_5$, which lead to a magnetically ordered ground state from within an intermediate valence scenario[4–6]. Specifically, we find a globally flat band consisting of Co *d* states near $E = -0.7$ eV, indicating the possibility of enhanced electronic and magnetic interactions in the "115" family of materials through localization in the Co layer, and we discuss a possible origin in geometric frustration. We also show that the delocalized Sm 4*f* states can hybridize directly with the Co $3d_{xz}/3d_{yz}$ orbitals, which occurs in our model at the Brillouin zone boundary point *R* in a band that is locally flat and touches the Fermi level from above. Our work identifies microscopic ingredients for additional magnetic interactions in the "115" materials beyond the RKKY mechanism, and strongly suggests that the Co *d* bands are an important ingredient in the formation of both magnetic and superconducting ground states.

The origin of heavy quasiparticles with *f* electron character is of fundamental interest due to their participation in unconventional superconductivity. In heavy fermion metals with a valence band of metallic *s*, *p*, and *d* electrons, the conduction electrons can turn into heavy quasiparticles by hybridizing with the localized *f* electrons. Hybridization of this type, involving the formation of entangled Kondo singlets that screen the *f* magnetic moments, has been observed in a variety of Ce-based intermetallics[1,3,7–14]. Microscopically, the Kondo hybridization mechanism depends on the details of the electronic wavefunctions, and it has been argued that hybridization is driven by the shape of the *f* orbital wavefunctions as they are determined by the crystal electric field[15,16].

The single-ion properties of Sm^{3+} ($4f^5$, $S = {}^5/_2$, $L = 5$, $J = {}^5/_2$) make it an analog of Ce^{3+} in $CeCoIn_5$ ($4f^1$, $S = {}^1/_2$, $L = 3$, $J = {}^5/_2$) with the same nominal *J*, while exhibiting similar single-ion properties, including the crystal field environment and atomic spin-orbit coupling. The case of $SmCoIn_5$ presents with predominantly localized *f* electrons, as well as an additional delocalized *f* component[6], similar to the case of $CeCoIn_5$. However, unlike $CeCoIn_5$, the ground state of $SmCoIn_5$ exhibits several antiferromagnetic (AF) ordered phases, with three phase transitions observed in specific heat at $T_{N,1} \approx 11$ K, $T_{N,2} \approx 8$ K, and $T_{N,3} \approx 6$ K[4,5]. Magnetic ordering in rare earth intermetallics is expected to be dominated by the RKKY mechanism[10,17,18]. In case of an additional Kondo hybridization, the RKKY interactions are reduced by the Kondo screening cloud, which typically prohibits the formation of long-range magnetic order. Therefore, the microscopic differences between $CeCoIn_5$ and $SmCoIn_5$, especially changes

[1]Laboratory for Neutron Scattering and Imaging, Paul Scherrer Institut, 5232 Villigen, Switzerland. [2]Laboratory for Materials Simulations, Paul Scherrer Institut, 5232 Villigen, Switzerland. [3]National Centre for Computational Design of Novel Materials (MARVEL), Paul Scherrer Institut, 5232 Villigen, Switzerland. [4]Photon Science Division, Paul Scherrer Institut, 5232 Villigen, Switzerland. [5]Laboratory for Multiscale Materials Experiments, Paul Scherrer Institute, 5232 Villigen, Switzerland. ✉e-mail: david-william.tam@psi.ch; michel.kenzelmann@psi.ch

in their most dominant magnetic interactions, may hold the key to understanding how magnetic ground states can emerge from within a system exhibiting Kondo screening.

To develop a microscopic picture of the Kondo screening environment in $SmCoIn_5$, we conducted ARPES measurements at T = 12 K and built an electronic structure model using DFT+U calculations. Our results confirm that $SmCoIn_5$ is dominated by the Sm^{3+} configuration[5,6] and is highly similar to other "115" materials, where the *f* electrons remain mostly localized and play only a small role in the overall characteristics of the band structure. Specifically, we find that the *f* electrons of Sm^{3+} sit near a binding energy of $E_B \approx 6$ eV, with good agreement between ARPES and our DFT+U results, showing little hybridization of the Sm^{3+} states. In addition, a second band of Sm states sits above this position by a value $E_B + U$, which happens to nearly overlap the Fermi energy E_F since $U \approx 6$ eV. We interpret this band loosely as an "upper Hubbard band" of Sm, because it comprises a situation where an *s*, *p*, *d* conduction electron tunnels onto the localized Sm^{3+} site, leading to an instantaneous Sm^{2+} configuration. To show that this picture is correct, we also conducted separate DFT calculations within a strictly Sm^{2+} configuration, which confirm that the Sm^{2+} states appear close to the Fermi energy (see supplementary information), although the details of that calculation also show that the Sm^{2+} configuration cannot be the ground state of $SmCoIn_5$. A partial Sm^{2+} character is also in agreement with previous experiments that show a slight admixture of the Sm^{2+} valence state at low temperatures below T = 60 K[6], similar to the intermediate valence state found in a variety of other Sm- and Yb-based materials[19–21]. Therefore, we believe the origin of the intermediate valence scenario in $SmCoIn_5$ is captured by our DFT calculations.

Looking in more detail, we first show (Figs. 1, 2 and 3) that the band structure observed by ARPES agrees very well with the DFT+U calculations, giving us a high degree of confidence in our model. The model reveals the "hot spots" in the Brillouin zone where the Sm *f* states hybridize with the conduction electrons near the Fermi energy E_F, and we find two spots of interest which we label $\gamma_Z = (0.25, 0, 0.2)$ and $R = 5, 0, 0.5)$ (Figs. 1c and 4). The γ_Z spot sits midway along the Γ-*X* cut direction with nonzero $k_z = 0.2$, which is similar to a large hot spot position previously found in ARPES, DFT, and DMFT studies of $CeCoIn_5$[1,3,12]. In $SmCoIn_5$, our model shows a smaller hot spot, which we argue may be related to the different single-ion properties of Ce^{3+} and Sm^{3+}.

The second "hot spot" for *f* hybridization in $SmCoIn_5$ is the high-symmetry *R* position (Figs. 3 and 4), located at the Brillouin zone boundary along both k_x and k_z, which was also previously identified as weakly important for $CeCoIn_5$[3] but more important for Sn-doped $CeCoIn_5$[13], which is in the limit of higher *f* electron itinerancy (higher E_F). Our model calculations (Figs. 3 and 4) unambiguously show that the *R* point contains only Sm-*f* and Co-*d* states, indicating that a direct hybridization mechanism is possible. Moreover, orbitally resolving the model (Fig. 5) shows that the *R* point contains only the Co $3d_{xz}$ orbital (or the equivalent $3d_{yz}$ orbital at the *R* point rotated 90 degrees about the origin). Since the *d*-*f* band is highly flat at the *R* point, it is likely that a large van Hove peak of Sm/Co states suddenly appears in the density of states, pinning the Fermi energy at the bottom of this band. The appearance of this singularity exactly at E_F suggests the *R* point plays a role in the ground state of $SmCoIn_5$, even though we do not observe it in our experiments. More importantly, due to the direct *f*-*d* hybridization within this band, our model shows generally that magnetic interactions of the Co *d* states can directly influence the magnetic degree of freedom of the heavy quasiparticles, whether through interactions at the $R = (0.5, 0, 0.5)$ wavevector or elsewhere.

Finally, our model shows unambiguously that a globally flat band appearing at $E = -0.7$ eV in $SmCoIn_5$, as well as in $LaCoIn_5$ and $CeCoIn_5$[1,2], consists of Co *d* states. Since our experiments and calculations both indicate that the band is globally flat, we suggest that the flatness of this band arises from a geometric frustration mechanism in the quasi-2D Co-In(2) layer. Specifically, we point out several square lattice models, including the checkerboard and Lieb lattices, that could apply to a subgroup of the Co *d* orbitals (see "Discussion"). Our results show microscopically that this flat band, where electronic and magnetic correlations are expected to be enhanced, can influence the heavy quasiparticles, either through direct exchange (such as at the R point) or via superexchange across the In(2) sites. We argue then that geometric frustration and the resulting flat *d* band may help explain the appearance of magnetic order within a system where the *f* states favor a delocalized ground state and, more broadly, that it might play an important (and until now overlooked) role in understanding magnetism and superconductivity in the "115" materials.

Results and discussion

Fermi surface and band structure of $SmCoIn_5$

Figure 1 shows the Fermi surface of $SmCoIn_5$ in the Γ-*X*-*M* and *Z*-*R*-*A* planes. ARPES intensity maps were taken as a function of the in-plane momentum (k_x, k_y) at the Fermi energy E_F using two photon energies corresponding to the Γ and *Z* points (Fig. 1d). Using the standard notation used for "115"s, e.g., of ref. 2, we observe three electron-like bands at the M point (α, β, and γ). The α and β sheets are visible around the M point with circular and cloverleaf shapes, respectively. The γ sheet is visible as parallel lines around the X point, as well as in some of the features close to Γ. In a DMFT study of $CeCoIn_5$, the γ sheet structure near X was shown to exhibit an in-plane curvature that pinches the pocket to a narrow point directly on the line between Γ and X. In $SmCoIn_5$, we observe that the γ sheet is highly parallel, with no in-plane curvature visible until the intersection of the β and γ pockets very close to the Γ point. The absence of such a pinch point suggests that the Sm *f* electrons do not enter the Fermi surface here, whereas they do in $CeCoIn_5$[3,12]. Instead, our model shows the *f* electrons in $SmCoIn_5$ only enter the Fermi surface at the γ_Z and *R* positions, as we discuss below. The absence of an in-plane hot spot might imply a more three-dimensional character to the Kondo screening in $SmCoIn_5$.

In Fig. 2, we show ARPES intensity maps (E_B-k_x) showing the band structure of $SmCoIn_5$ along high-symmetry cuts between E_F and binding energy $E_B = 7$ eV. The flat band near $E_B = -5.6$ eV is from Sm^{3+}, and its flatness reflects the predominantly localized nature of Sm^{3+}, wherein the *f* electrons cannot hybridize strongly. The band structure near E_F is accurately captured by our DFT calculations in minute detail, as shown in Fig. 3. In Fig. 3a, c, e, we zoom into the band structure near E_F along the same high-symmetry cuts adopted in Fig. 2. Around the *M* point, shown in Fig. 3c, d, electronic-like α, β, and γ sheets are highly consistent with the band structure of $LaCoIn_5$ and $CeCoIn_5$[1,2]. At the Brillouin zone boundary at *Z*, shown in Fig. 3e, f, the γ sheet creates an open pocket at E_F near *Z*, while the lower δ sheet is closed at both Γ and Z and exhibits an inversion from concave down to concave up between Γ and *Z*. In a previous ARPES study of $CeCoIn_5$[12], it was reported that depending on the surface termination, some bulk features could appear in different layers of the experimental data. In our data, we observe such an extra band in the Γ-*X*-Γ cut (Fig. 3b, about 0.2 eV above the δ band and forming an open pocket at Γ), which closely resembles the γ sheet that is found by our bulk DFT calculations only along the *Z*-*R*-*Z* cut (Fig. 3e, f). Since this is precisely the same termination state proposed for a Ce-In(1) surface in $CeCoIn_5$ (cf. Fig. 2a of ref. 12), we attribute this feature in our data to a 2D termination state containing the Sm-In(1) crystallographic layer.

In all cuts shown in Figs. 2 and 3, we observe the presence of a very strong and flat band near $E - E_F = -0.7$ eV, which we label with the archaic Greek letter Ϝ (digamma). A similar flat band was also observed in $LaCoIn_5$ and $CeCoIn_5$[1,2], but it was not clearly determined if this band arises from an ionization state of the localized rare earth ion, or if it is part of the *p* and *d* metallic bands. From our DFT calculations on $SmCoIn_5$, we can confirm that the origin of this flat band is from Co 3*d* orbitals, as can be seen in the density of states in Fig. 3a, c, e, shown on the right side of each sub-panel. By comparing the experimental ARPES data to the calculations in Fig. 3b, d, f, we note several unusual properties of the Ϝ band. Firstly, its strong intensity (on par with the Sm flat band at $E - E_F = -5.6$ eV), overall flatness throughout the Brillouin zone, and lack of any observable hybridization points (anti-crossings) with any other metallic band, suggests that it represents a significant and relatively isolated subsystem of Co *d* states.

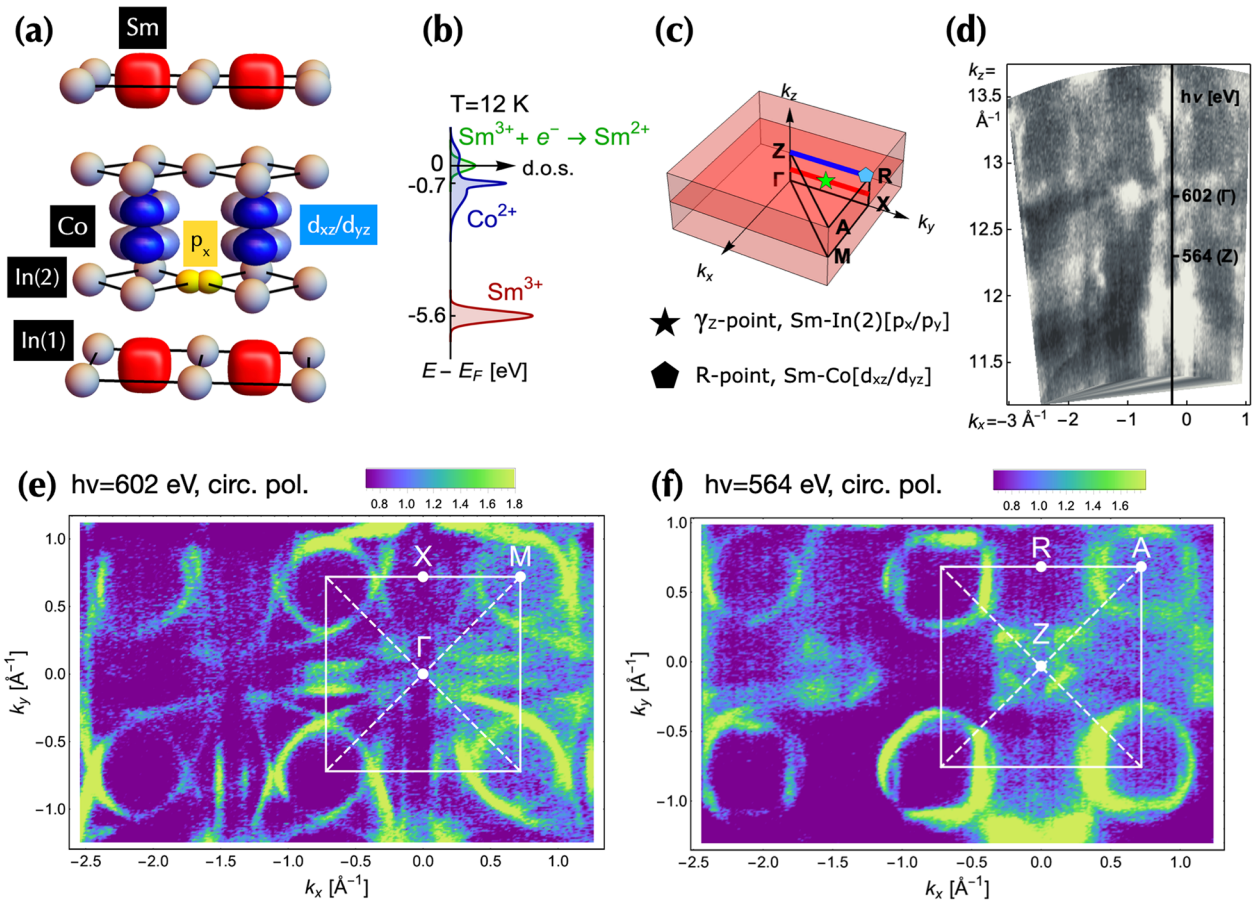

Fig. 1 | Orbital configuration and Fermi surface of $SmCoIn_5$. a Tetragonal unit cell of $SmCoIn_5$, showing the position and orientation of the In(2) p_x orbital (yellow) and Co d_{xz}/d_{yz} orbitals (light and dark blue, respectively). **b** Sketch of the density of states of $SmCoIn_5$ relative to E_F. **c** Conventional labels within the *P*4/*mmm* Brillouin zone, highlighting two positions of interest γ_Z (k = [0.25, 0, 0.2]) and R (k = [0.5, 0, 0.5]). **d** ARPES intensity at T = 12 K, parallel to the Γ-*X* direction, while varying photon energy $h\nu$, demonstrating the coupling of photon energy to the out-of-plane k_z direction and identifying the energies corresponding to two high-symmetry planes along the k_z axis. **e** Fermi surface of $SmCoIn_5$ in the Γ-*X*-*M* plane (k_z = 0) using circularly polarized light with photon energy $h\nu$ = 602 eV, and **f** *Z*-*R*-*A* plane ($k_z = \pi$) using circularly polarized light with photon energy $h\nu$ = 564 eV.

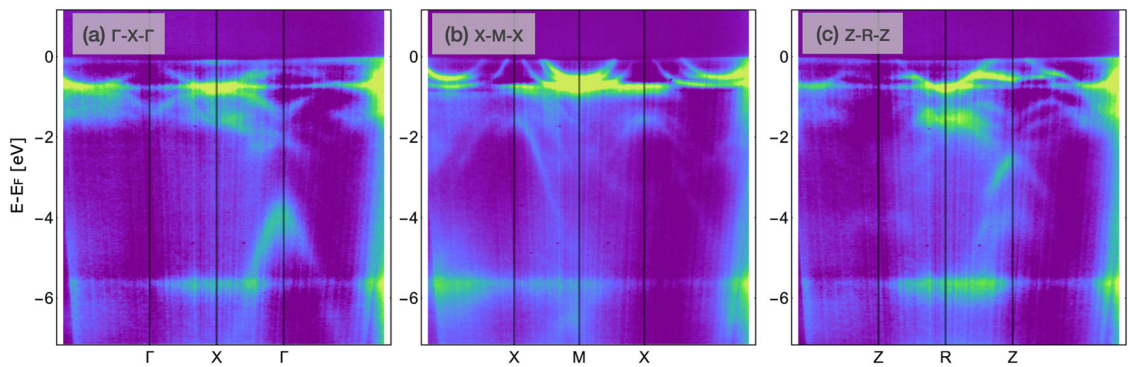

Fig. 2 | ARPES E_B-k_x maps showing the band structure of $SmCoIn_5$. a Γ-*X*-Γ cut for $E-E_F > -7$ eV. The data has been partially background-subtracted using a line-derivative method in order to enhance the visibility of the bands. **b** *X*-*M*-*X* cut. **c** *Z*-*R*-*Z* cut.

Second, we note the possibility that the band is even flatter than the model calculations predict, which would indicate the presence of electronic correlations in the *d* band beyond the DFT+U level of approximation. The flat band may arise from geometric frustration in a sublattice of Co orbitals, as we show in the following sections, and therefore give rise to additional magnetic interactions. Moreover, since the Co *d*-shell is unfilled and therefore has a magnetic degree of freedom, the ϝ band can additionally couple magnetically to the entangled Kondo states, which are magnetic singlets. In general, the presence of the ϝ band shows that strong correlations in the *d* states can directly influence the magnetic properties of the heavy quasiparticles near E_F.

Hybridization points between *f* states and metallic bands

To understand the details of the hybridization between Sm *f* electrons and the other bands, we projected our DFT calculations into the basis of different atomic shells and studied the "hot spots" near the Fermi energy that contain

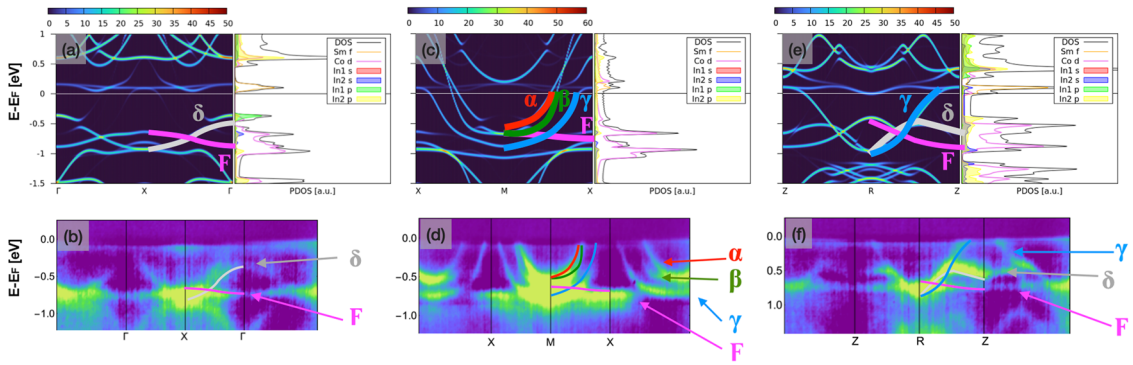

Fig. 3 | Comparison between DFT+U model calculations and ARPES within 1 eV of E_F. **a** DFT calculated band structure and density of states along the Γ-*X*-Γ cut, and **b** comparison with ARPES data that has been enhanced using the background subtraction method of Fig. 2. The lines that are drawn in by hand over the DFT panel are copied directly onto the ARPES panel below, signifying good agreement, and the colored labels specify the band names discussed in the text. Note that the colors of these bands are not related to the colors indicated in the density of states plots on the right-hand side of each DFT plot. **c**, **d** *X*-*M*-*X* cut. **e**, **f** *Z*-*R*-*Z* cut.

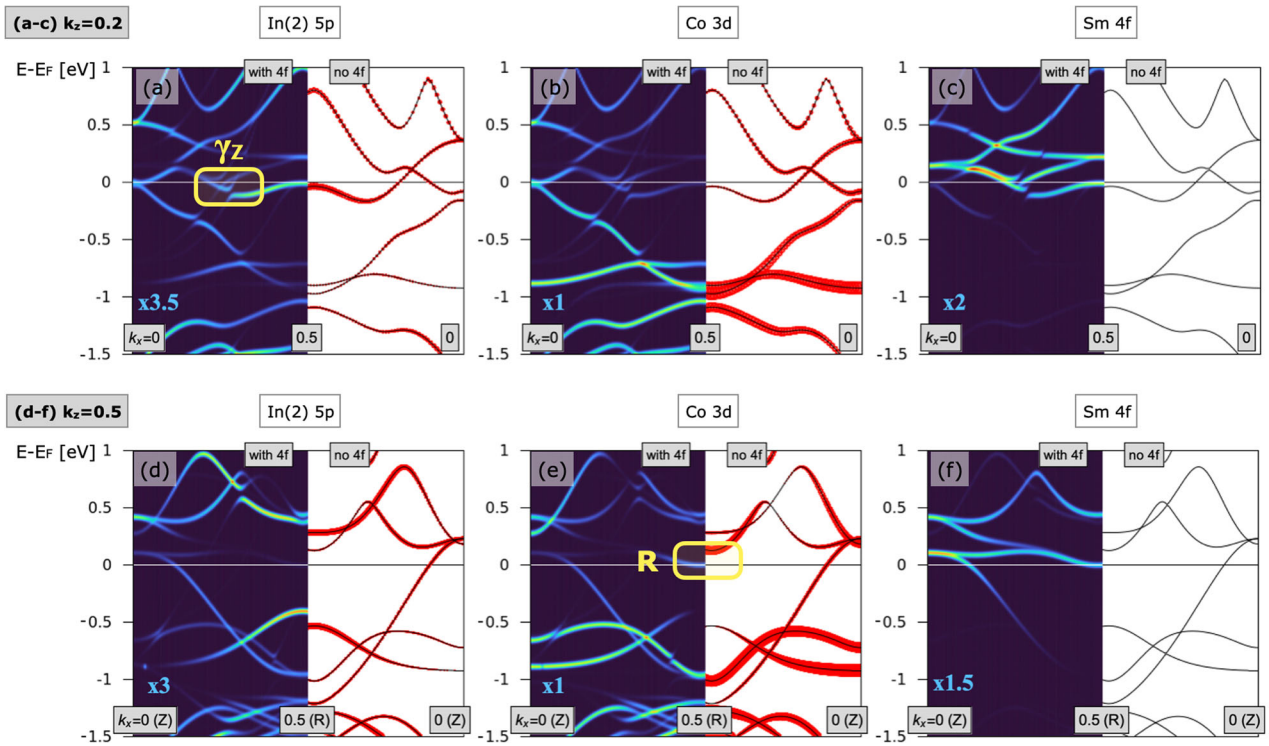

Fig. 4 | Atomically resolved DFT calculated band structure of $SmCoIn_5$ parallel to the Γ-X-Γ high-symmetry cut. **a**–**c** $k_z = 0.2$ and **d**–**f** $k_z = 0.5$ (*Z*-*R*-*Z*). Panels (**a**, **d**) show spectral weight of the In(2) site 5*p* orbitals, (**b**, **e**) show Co 3*d*, and (**c**, **f**) show Sm 4*f*. Each sub-panel shows our calculations for $SmCoIn_5$ (left side) along with a nonmagnetic calculation with the 4*f* electrons frozen in the core (right side). In the left sub-panels, the intensity of the bands is proportional to the specific atomic orbital content of each band, and is multiplied by the scale factor written in light blue at the bottom of the plot. For example, in panel (**a**), the band colors for In(2) 5p have been multiplied by a factor 3.5 compared to the density of Co 3*d* states in panel (**b**). For the nonmagnetic calculations in the right sub-panels, the specific orbital content is proportional to the thickness of the red lines superimposed on the bands. The differences between the magnetic and nonmagnetic calculations is evidenced by slight changes to the position of the bands due to the presence of Sm *f* electrons. Two "hot spots" of interest at γ_Z and *R* (highlighted in panels (**a**) and (**e**)) show a large density of Sm 4*f* states, as shown in panel (**c**) and panel (**f**). In the supplementary information, we additionally show similar plots with projections into the In(1) 5s, In(1) 5p, and In(2) 5s orbitals.

Sm states. In Fig. 4, we show projections along two high symmetry cuts parallel to the Γ-*X*-Γ direction, for $k_z = 0.2$ (a–c) and $k_z = 0.5$ (d–f), both with $k_y = 0$. In panel (a), we use a yellow box to highlight the γ_Z hot spot position $k = (0.25, 0, 0.2)$, which contains significant Sm weight (panel (c)). We find that the In (2) 5*p* orbitals dominate the shallow band extending from γ_Z up to $k_x = 0.5$ (the *X* point), while the γ_Z position itself contains a mixture of In (1) and In (2) states, with the In (2) 5*p* states providing the largest contribution (contributions from the other orbitals In[1] 5s, In[1] 5p, and In[2] 5s are shown in the supplementary information). The existence of Sm states near the *X* point below E_F represents another difference between $CeCoIn_5$ and $SmCoIn_5$.

From both the model calculations and experimental data, the $\gamma_Z = (0.25, 0, 0.2)$ hot spot in $SmCoIn_5$ is smaller and more isolated compared to $CeCoIn_5$. Specifically, we find no evidence that the *f* states at γ_Z are

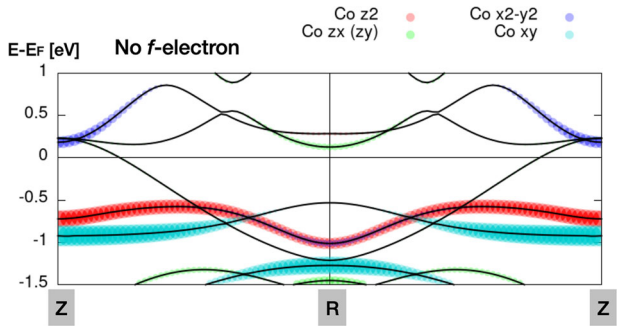

Fig. 5 | Orbital-resolved Co 3*d* orbitals from a DFT calculation of $SmCoIn_5$ with *f* electrons frozen into the core. The orbitals hybridizing with Sm *f* states are found to be $d_{x^2-y^2}$ at *Z*, and d_{xz}/d_{yz} at *R*. The flat ϝ band contains d_{xy} and d_{z^2}.

distributed over the larger *Z*-centered Fermi surface pocket at E_F (see Supplementary Fig. 4g; cf. ref. 3), and we find no significant *f* contributions in the middle of the *Z*-*R* cut (Fig. 4f; cf. refs. 37). Instead, our DFT+U model shows that the states near the *Z* point are dominated by the conduction electrons, and we find no experimental evidence of any deviations from the model along the *Z*-*R*-*Z* cut that would show the presence of *f* states. However, we have retained the notation γ_Z in this work to refer to the hybridization hot spot (0.25, 0, 0.2), and to avoid confusion with the Fermi surface γ sheet. The observation of a small γ_Z hot spot in $SmCoIn_5$ could be related to different hybridization conditions between the relatively anisotropic Ce^{3+} ground state wavefunctions[15,16], compared to the highly isotropic wavefunctions of Sm^{3+} [6]. The lower anisotropy would also explain why a DFT+U approach results in a very realistic model for $SmCoIn_5$ without the need to take into fully account for the effects of the small crystal field splitting of the lowest *f* manifold, which is beyond a mean-field approach. Our model shows that the γ_Z position hybridizes slightly with the 5*s* and 5*p* orbitals of both In sites, but is dominated by Sm^{3+} spectral weight. Since the In(2) site was also shown to have a strong effect on the ground state superconductivity in Ce-based "115" compounds[7,16], we show the In(2) character in Fig. 4 while noting that there is an admixture of other orbitals at γ_Z. Within the In(2) atom, we find the most important contribution is from the $5p_x$ orbital (or with the equivalent $5p_y$ orbital at the position rotated 90 degrees about the origin), as is expected from the shape of the $5p_x$ orbitals.

Turning to the hot spot at the *R* point $k = (0.5, 0, 0.5)$, in Fig. 4d–f we show the presence of a shallow band which appears pinned to the Fermi level and consists of Co *d* and Sm *f* states. This *R*-centered hot spot does not appear to be smoothly connected to the γ_Z hot spot, but is instead a separate feature with a distinct set of associated quasiparticles. In Supplementary Fig. 4, we show constant-energy slices plotting k_z against k_x, which show that two minima can be clearly distinguished from one another up to energies at least 20 meV above E_F. Furthermore, the absence of In(2) states in this band (Fig. 4d) shows that the Sm and Co states exhibit magnetic coupling through a direct exchange mechanism, which is relevant not only for this locally flat band at *R*, but also more generally shows that direct exchange can be achieved between the rare earth and transition metal electrons in the "115" materials. Since the *d*+*f* band at *R* is very shallow, spanning nearly ~ 0.2 reciprocal lattice units before deviating significantly from $E = E_F$, the *R* point allows a flat band of *d* states to directly hybridize with the heavy *f* quasiparticles. Moreover, the local flatness of this band suggests that the van Hove singularity in the density of states is responsible for pinning the Fermi energy to the bottom of this band at *R*. Therefore, although Sm *f* states are already present at γ_Z at energies below E_F, we find that the hybridized flat band at *R* is probably touching the Fermi energy.

To further study how hot spots develop at the γ_Z and *R* hot spots, we conducted separate DFT calculations with the *f* electrons frozen into the core, shown on the right side of each sub-panel in Fig. 4. Qualitatively, the two calculations are highly consistent, although one important difference is at the *R* point, where the Co *d* band does not dip down low enough to reach E_F in the nonmagnetic case, showing that the interaction between Sm and Co states is the driving mechanism behind creating an interaction between Sm and Co at *R*. Since the nonmagnetic calculations do not require the use of a magnetic supercell, we also use them to show the proper projection of the In and Co bands onto the orbitals within the crystallographic unit cell illustrated in Fig. 1a. In the case of the γ_Z position (see Supplementary Information), we find that the In(2) $5p_x$ orbital dominates the shallow band between $k_x = 0.3$ and 0.5 where the Sm*f* states occur, while exactly at γ_Z it is still the most important of the *s*, *p*, *d* orbitals but by a smaller margin. Hence, quasiparticles at γ_Z exhibit largely Sm-Sm interactions, and could support a Fermi surface nesting instability between neighboring γ_Z points—e.g., with wavevector $q = (0.5, 0, 0.4)$—driven by the Sm electrons. On the other hand, at the *R* point, shown in Fig. 5, we find that the d_{xz} orbital completely dominates the *d*+*f* band at E_F. This result shows that the hybridization between Sm and Co at *R* is orbitally selective, such that the interactions affecting the heavy quasiparticles there are related to the symmetry of the Co d_{xz}/d_{yz} orbitals. In the magnetically ordered ground state of $SmCoIn_5$[4,5], zone folding and reconstruction of the electronic bands may further increase the weight of the *R* point below E_F. Therefore, from a magnetic point of view, the orbital-selective magnetic exchange pathways in $SmCoIn_5$ involving the d_{xz}/d_{yz} orbitals may be an important mechanism competing with Sm-Sm interactions, with consequences for the magnetically ordered ground state of the Sm sublattice.

Localization in the Co layer of "115" materials

In our DFT+U calculations, the density of states of the Co 3*d* electrons appears predominantly between E_F and about $E_B = 3$ eV, and exhibits a strong flat band (ϝ) near $E = -0.7$ eV. Flat bands in general are hosts of electronic localization (e.g., refs. 22,23), and they have been previously shown to have a strong effect on magnetic ground states in transition metal systems[24–29]. Moveover, since our ϝ band is globally flat throughout the entire Brillouin zone, we are inclined to search for explanations in terms of a robust symmetry-protected mechanism. To this end, flat bands arising from geometric frustration have been identified in a variety of square or square-like lattices[30–37], many of which can also host unconventional superconductivity, posing a deeper connection between the ϝ band and the phenomenology of the 115s.

If the ϝ band is globally flat because of geometric frustration, analysis of the 115 crystal structure can elucidate how this occurs. In the 115 structure, Co atoms occupy a square lattice. Therefore, one possibility is that the band structure of the 115s hosts a very specific hierarchy of couplings involving the square lattice, such as the checkerboard lattice proposed in[30]. On the other hand, as we show in Fig. 1a, the Co site is also coordinated by four In(2) sites just above the plane of Co, and four below. This Co-In(2) sublattice bears a resemblance to the Lieb lattice, a bipartite square lattice where the central site of the square is coordinated by four neighbors of another species. Phenomenologically, studies of the Hubbard model on the Lieb lattice have focused on its relationship with both magnetism[32,38,39] and superconductivity[31,33], including as a model for orbital selective superconductivity in the cuprates[35]. Since both checkerboard and Lieb lattice models also contain the ingredients for topologically nontrivial band crossings[30,37,40], the ϝ band may be important to the 115s in yet another way, since such a crossing was previously proposed in a study of $CeCoIn_5$[41]. In general, the possibility of a specific square lattice model or a Lieb lattice model shows that $SmCoIn_5$ can easily contain the ingredients for geometric frustration in the square-like sublattice of Co *d* states.

The appearance of geometric frustration does not necessarily imply that the ground state of the frustrated sublattice is the ground state of $SmCoIn_5$. Since the ϝ band in the 115s is not situated at the Fermi energy, its quasiparticles are not thermally activated. However, since the Co *d*-shell is partially unfilled, the magnetic interactions within the ϝ band can nevertheless directly influence the itinerant quasiparticles. Also, as we have shown in $SmCoIn_5$, direct hybridization can occur between heavy quasiparticles with specific Co *d* orbitals (in our model, with d_{xz}/d_{yz} at the *R*-point), proving that the effects of the Co flat band can be felt directly by the partly

delocalized *f* states. Therefore, in $CeCoIn_5$, where the delocalized *f* states participate in a superfluid condensate, interactions arising from the Γ band of *d* states might also influence the superconducting pairing mechanism.

f-Multiplet-driven hybridization

In a DMFT study of $CeCoIn_5$, different multiplets of the Ce *f* electrons were shown to selectively hybridize with the β band between *X* and *M*, and with the γ band between Γ and *X*[3]. With the much richer multiplet structure of Sm[6,42], the hybridization in Sm is more complex, and may contain charge-like degrees of freedom in addition to the typical magnetic Kondo hybridization[6]. In addition to the spin-orbit coupling, which splits the Sm *f* levels into multiplets with different *J*, the multi-*f*-electron configuration in Sm also contains Coulomb repulsion between *f* electrons, a situation not present in the single-*f*-electron case of Ce. This additional term couples multiplets of different *J*, leading to a vastly larger subspace of *f* multiplet levels compared to the case of Ce, which is limited to just 14 *f* states with definite splittings set by the single-ion properties. Therefore, with Sm it is possible for even a tiny amount of curvature in a nominally flat band to encompass many multiplet states of the Sm ion. For example, within 0.3 eV of E_F, the ground state of Ce^{3+} contains the 14 multiplet levels of different m_J, whereas Sm^{3+} exhibits nearly 200 different levels that are mixtures of different *J* and m_J[6]. Significantly, the various multiplets may have different Kondo coupling strengths that exhibit different hybridization strengths with the itinerant valence band electrons. This dramatically increases the likelihood of a Kondo-like interaction between at least one of the multiplet states with the valence band, at an energy close enough to E_F to exhibit a Kondo resonance. The large subspace of *f* levels in a multi-*f*-electron system may therefore present a natural explanation for why many Sm-based materials exhibit high effective masses[19], and is of particular interest in cases such as $SmCoIn_5$ where the Sm/Co *d*+*f* band is already locally flat at the *R* point. It would therefore be interesting to conduct further photoemission studies on $SmCoIn_5$ or doped $SmCoIn_5$ with high resolution, which could possibly show if *f* multiplet wavefunctions other than the ground state are directly involved in the Kondo coupling, a complexity less likely to be encountered in Ce-based materials.

Magnetic exchange

Finally, we address the magnetic exchange in the Sm-Sm, Sm-Co, and Co-Co subsystems. In the tetragonal lattice structure of $SmCoIn_5$, the Sm and Co atoms both form two-dimensional square lattices parallel to the basal *ab* plane, as shown in Fig. 1a, b. The Sm and Co layers alternate along the *c* axis with a direct stacking structure, such that a Co atom sits directly between two Sm atoms. The nearest neighboring Sm atoms in the *ab* plane are separated by the *a* lattice parameter of 4.5 Å and contain an In(1) ion in the same plane, while the In(2) ions sit between the Sm and Co layers. If the Sm and Co ions have a direct magnetic exchange pathway between them, it could also involve the In(2) sites, which could create a magnetic superexchange-like interaction. An interaction involving In(2) is plausible because the wavefunction shapes of the Co d_{xz}/d_{yz} orbitals lie closest to the In(2) sites, as shown in Fig. 1a, b. Depending on the details of hybridization with the In(2) p_x, p_y, or p_z orbitals, the magnetic superexchange mechanism could support multiple pathways with different ferromagnetic (FM) or antiferromagnetic (AF) exchange constants, in addition to the in-plane exchange pathway coupling Sm to Sm across the In(2) p_x orbital. Therefore, the In(2) site may provide another degree of freedom in tuning the magnetic exchange pathway between Sm and Co, and through it, the proportion of heavy quasiparticles entering the Fermi surface at the γ_Z point versus those entering at *R*. Since it was previously shown that hybridization between the rare earth and In(2) site is an important factor in controlling superconductivity in the $CeCoIn_5$-$CeRhIn_5$-$CeIrIn_5$ series[15,16], the complexity of the interactions that we observe in $SmCoIn_5$ may hold a key to understanding the origin of the ground state. Specifically, the existence of competing magnetic exchange pathways involving the rare earth (R) sites, specifically, R-In(2)-R (in plane), R-Co-R (out of plane), and R-In(2)-Co-In(2)-R, may have consequences for how magnetic and/or superconducting ground states form in the 115s.

In addition to the RKKY mechanism, the role of direct magnetic exchange and magnetic superexchange can be generally important for *d* and *f* electrons in rare earth intermetallics. For instance, in $(La,Tb)Mn_2Si_2$, it was proposed that an R-Mn-R interlayer superexchange mechanism is responsible for stabilizing AF order, while the Si atoms could act as mediators for superexchange between neighboring planes of Mn atoms along the *c* axis[43,44]. In $SmCoIn_5$, hybridization of the Sm *f* and Co *d* orbitals, possibly involving superexchange across the In(2) sites, suggests that these exchange mechanisms have more than one way to affect the magnetic Hamiltonian, particularly along the *c*-axis. Such magnetic exchange pathways would therefore compete with the RKKY mechanism, and could play a destabilizing role in the magnetic ground state, particularly for interactions along the *c* axis. Competition between these magnetic interactions may therefore help explain the complicated magnetic phase diagram of $SmCoIn_5$[5]. Therefore, our observation of flat *d* bands interacting with states near the Fermi energy suggests a mechanism for FM and AF interactions to compete in $SmCoIn_5$ beyond the RKKY model, and also suggests that because of this competition, fine tuning by strong correlation effects among the *d* states may have an outsize effect on the ultimate ground state of the material and the ordered structure of Sm local moments.

Summary

In summary, close agreement between ARPES measurements and DFT+U calculations shows that the band structure of $SmCoIn_5$ exhibits coupling of the localized Sm *f* states at the Fermi level via hybridization with specific In 5*p* and Co 3*d* metallic states. Our model shows that heavy quasiparticles containing Sm *f* character can hybridize at multiple positions in the Brillouin zone, including a position supporting Sm-In(2)[$5p_x$] hybridization that is similar to previous results on $CeCoIn_5$, and a second position at the zone boundary supporting Sm-Co[$3d_{xz}$] hybridization (simultaneously with the equivalent orbitals $5p_y$ and $3d_{yz}$, respectively, along the other in-plane direction in the crystal). Meanwhile, the Co *d* orbitals exhibit a globally flat band (Γ), which has a likely origin in geometric frustration.

The magnetic interactions arising from coupling of the itinerant quasiparticles to the Co layer, whether through direct hybridization (e.g., at *R*), through mean field interactions (because of a partly unfilled Co *d* shell), or through superexchange interactions involving the In(2) sites, all point to the importance of the Co *d* states in determining the ground state. Since the *d* shell is common to all "115" materials, electronic localization may play an overlooked role in the ground states found in this family, including unconventional superconductivity. In $SmCoIn_5$, the delocalized nature of Sm states at the hot spots shows how magnetic interactions can go beyond the typical RKKY mechanism, and may explain why the Sm *f* states in $SmCoIn_5$ exhibit both a delocalized component and localized magnetic order.

Methods

Sample growth

$SmCoIn_5$ single crystals were grown using an indium flux method that we described previously[6]. Crystals were separated from the flux by centrifugation and later etched in hydrochloric acid. The $SmCoIn_5$ samples exhibited a plate-like habit corresponding to the basal plane of the crystal.

ARPES experiments

Angle-resolved photoemission spectroscopy (ARPES) experiments were carried out at the soft-x-ray endstation[45] of the ADRESS beamline[46] at the Swiss Light Source, PSI, Switzerland. Single crystals were mounted using the natural basal plane on copper plates using high-strength H20E silver epoxy. Posts made of small stainless steel screws were attached onto the top surfaces of the samples with Torr-Seal epoxy. The samples were cleaved in ultrahigh vacuum of about 10^{-10} mbar. We used circularly polarized light with a beam spot of about 60 × 100 μm on the sample. We determined the coupling of beam energy to the out-of-plane k_z direction by scanning the beam energy over $h\nu$ = 480 to 700 eV, shown in Fig. 1d. We identified $h\nu$ = 602 eV as the energy where the in-plane iso-E_B maps correspond to the Γ-*X*-*M* plane, and

$h\nu = 564$ eV as the energy corresponding to the *Z-R-A* plane. The use of soft-x-ray photon energies results in large photoelectron mean free paths, and the latter translates, by the Heisenberg relation, to sharp definition of the out-of-plane momentum k_z[47,48]. Maps as a function of two-dimensional in-plane momentum (k_x, k_y) were then collected at these energies to observe the Fermi surface and band structure, where we found broad similarity to published results of $CeCoIn_5$ that use DFT[1,12] and dynamical mean-field theory[3].

DFT calculations

All the density functional theory (DFT) calculations were carried out using the Quantum ESPRESSO package[49–51]. Exchange and correlation effects were modeled using the PBEsol functional[52], augmented by a Hubbard U term to better describe the physics of the localized Sm 4*f* electrons. The scalar-relativistic pseudopotentials are taken from the SSSP library[53]. To sample the Brillouin zone, we used a $7 \times 7 \times 7$ Monkhorst-Pack grid, a $10 \times 10 \times 10$ grid was used for the calculation of the projected density of states. The wavefunctions (charge densities and potentials) were expanded using a kinetic energy cutoff of 70 Ry (560 Ry). We used the experimental lattice constants and internal atomic positions[54,55] throughout this work. The values of U used in this work (U = 6.18 eV and U = 6.26 eV for Sm^{3+} and Sm^{2+} calculations, respectively) were computed fully ab initio by using the linear response approach[56] as implemented in refs. 57,58. In order to "nudge" the self-consistent-field calculations to converge to the Sm^{3+} solution, we prepared the systems in initial configurations that have 5 electrons in the Sm *f* shell. Some of these initial configurations eventually converge to a self-consistent solution that exhibit the desired 3^+ oxidation state for the Sm atoms. At the level of DFT+U this solution is always metastable, i.e., its energy is slightly higher then that of the Sm^{2+} (6 electrons in the Sm *f* shell) solution. However, it is the one that best reproduces the ARPES data. Also, we did not use any +U corrections for the Co 3*d* states as this deteriorates the agreement with the ARPES data. Finally, in the magnetic calculations including the *f* electrons, the unfolding of the bands in the 7-atom Brillouin zone was performed using the unfold-x code (https://bitbucket.org/bonfus/unfold-x/src/master/)[59].

Data availability

The data used to produce the simulation results presented in this work are available at the Materials Cloud Archive[60]. Experimental datasets are available from the corresponding author on reasonable request.

Received: 25 July 2023; Accepted: 9 February 2024;
Published online: 14 March 2024

References

1. Chen, Q. Y. et al. Direct observation of how the heavy-fermion state develops in $CeCoIn_5$. *Phys. Rev. B* **96**, 045107 (2017).
2. Chen, Q. Y. et al. Electronic structure study of $LaCoIn_5$ and its comparison with $CeCoIn_5$. *Phys. Rev. B* **100**, 035117 (2019).
3. Jang, S. et al. Evolution of the Kondo lattice electronic structure above the transport coherence temperature. *PNAS* **117**, 23467–23476 (2020).
4. Inada, Y., Hedo, M., Fujiwara, T., Sadamasa, T. & Uwatoko, Y. Physical properties of $SmMIn_5$ (M=Co, Rh, Ir). *Phys. B: Condens. Matter* **378–380**, 421–422 (2006).
5. Pouse, N. et al. Temperature versus Sm concentration phase diagram and quantum criticality in the correlated electron system $Ce_{1-x}Sm_xCoIn_5$. *Phys. Rev. B* **97**, 235149 (2018).
6. Tam, D. W. et al. Charge fluctuations in the intermediate-valence ground state of $SmCoIn_5$. *Commun. Phys.* **6**, 1–11 (2023).
7. Shim, J. H., Haule, K. & Kotliar, G. Modeling the localized-to-itinerant electronic transition in the heavy fermion system $CeIrIn_5$. *Science* **318**, 1615–1617 (2007).
8. Fujimori, S. et al. Direct observation of a quasiparticle band in $CeIrIn_5$: an angle-resolved photoemission spectroscopy study. *Phys. Rev. B* **73**, 224517 (2006).
9. Koitzsch, A. et al. Observing the heavy fermions in $CeCoIn_5$ by angle-resolved photoemission. *Phys. C: Supercond. Appl.* **460–462**, 666–667 (2007).
10. White, B. D., Thompson, J. D. & Maple, M. B. Unconventional superconductivity in heavy-fermion compounds. *Phys. C: Supercond. Appl.* **514**, 246–278 (2015).
11. Patil, S. et al. ARPES view on surface and bulk hybridization phenomena in the antiferromagnetic Kondo lattice $CeRh_2Si_2$. *Nat. Commun.* **7**, 11029 (2016).
12. Kurleto, R. et al. Photoemission signature of momentum-dependent hybridization in $CeCoIn_5$. *Phys. Rev. B* **104**, 125104 (2021).
13. Maksimovic, N. et al. Evidence for a delocalization quantum phase transition without symmetry breaking in $CeCoIn_5$. *Science* **375**, 76–81 (2022).
14. Xu, C., Cao, C. & Zhu, J.-X. Pressure-induced concomitant topological and metal-insulator quantum phase transitions in $Ce_3Pd_3Bi_4$. *npj Quantum Mater.* **7**, 1–5 (2022).
15. Willers, T. et al. Crystal-field and Kondo-scale investigations of $CeMIn_5$ (M = Co, Ir, and Rh): a combined x-ray absorption and inelastic neutron scattering study. *Phys. Rev. B* **81**, 195114 (2010).
16. Willers, T. et al. Correlation between ground state and orbital anisotropy in heavy fermion materials. *PNAS* **112**, 2384–2388 (2015).
17. Čermák, P. et al. Magnetic structures of non-cerium analogues of heavy-fermion Ce_2RhIn_8: case of Nd_2RhIn_8, Dy_2RhI_{n8} and Er_2RhIn_8. *Phys. Rev. B* **89**, 184409 (2014).
18. Mazzone, D. G. et al. Evolution of magnetic order from the localized to the itinerant limit. *Phys. Rev. Lett.* **123**, 097201 (2019).
19. Higashinaka, R., Yamada, A., Matsuda, T. D. & Aoki, Y. Relationship between specific heat, valence and effective magnetic moment of Sm ions in strongly correlated Sm compounds. *AIP Adv.* **8**, 125017 (2018).
20. Kummer, K. et al. Similar temperature scale for valence changes in Kondo lattices with different Kondo temperatures. *Nat. Commun.* **9**, 2011 (2018).
21. Liu, H. et al. f-electron hybridised Fermi surface in magnetic field-induced metallic YbB12. *npj Quantum Mater.* **7**, 1–7 (2022).
22. Tang, L. et al. Photonic flat-band lattices and unconventional light localization. *Nanophotonics* **9**, 1161–1176 (2020).
23. Puntel, D. et al. Photoinduced dynamics of flat bands in the kagome metal CoSn. Preprint at http://arxiv.org/abs/2305.09531 (2023).
24. Melzi, R. et al. $Li_2VO(Si, Ge)O_4$, a prototype of a two-dimensional frustrated quantum Heisenberg antiferromagnet. *Phys. Rev. Lett.* **85**, 1318–1321 (2000).
25. Melzi, R. et al. Magnetic and thermodynamic properties of Li_2VOSiO_4: a two-dimensional S = 1/2 frustrated antiferromagnet on a square lattice. *Phys. Rev. B* **64**, 024409 (2001).
26. Lin, Z. et al. Flatbands and emergent ferromagnetic ordering in Fe_3Sn_2 kagome lattices. *Phys. Rev. Lett.* **121**, 096401 (2018).
27. Li, Y. et al. Flat-band magnetism and helical magnetic order in Ni-doped $SrCo_2As_2$. *Phys. Rev. B* **100**, 094446 (2019).
28. Yin, J.-X. et al. Negative flat band magnetism in a spin-orbit-coupled correlated kagome magnet. *Nat. Phys.* **15**, 443–448 (2019).
29. Kang, M. et al. Topological flat bands in frustrated kagome lattice CoSn. *Nat. Commun.* **11**, 4004 (2020).
30. Sun, K., Gu, Z., Katsura, H. & Das Sarma, S. Nearly flatbands with nontrivial topology. *Phys. Rev. Lett.* **106**, 236803 (2011).
31. Iglovikov, V. I., Hébert, F., Grémaud, B., Batrouni, G. G. & Scalettar, R. T. Superconducting transitions in flat-band systems. *Phys. Rev. B* **90**, 094506 (2014).
32. Noda, K., Inaba, K. & Yamashita, M. Magnetism in the three-dimensional layered Lieb lattice: enhanced transition temperature via flat-band and Van Hove singularities. *Phys. Rev. A* **91**, 063610 (2015).
33. Julku, A., Peotta, S., Vanhala, T. I., Kim, D.-H. & Törmä, P. Geometric origin of superfluidity in the lieb-lattice flat band. *Phys. Rev. Lett.* **117**, 045303 (2016).

34. Nunes, L. H. C. M. & Smith, C. M. Flat-band superconductivity for tight-binding electrons on a square-octagon lattice. *Phys. Rev. B* **101**, 224514 (2020).
35. Yamazaki, K. et al. Superconducting mechanism for the cuprate $Ba_2CuO_{3+\delta}$ based on a multiorbital Lieb lattice model. *Phys. Rev. Res.* **2**, 033356 (2020).
36. Xu, F., Zhang, L. & Jiang, L.-Y. Temperature and doping dependent flat-band superconductivity on the Lieb-lattice. *Chin. Phys. B* **30**, 067401 (2021).
37. Fan, R., Sun, L., Shao, X., Li, Y. & Zhao, M. Two-dimensional Dirac materials: tight-binding lattice models and material candidates. *ChemPhysMater* **2**, 30–42 (2023).
38. Tasaki, H. From Nagaoka's ferromagnetism to flat-band ferromagnetism and beyond: an introduction to ferromagnetism in the Hubbard model. *Prog. Theor. Phys.* **99**, 489–548 (1998).
39. Noda, K., Koga, A., Kawakami, N. & Pruschke, T. Ferromagnetism of cold fermions loaded into a decorated square lattice. *Phys. Rev. A* **80**, 063622 (2009).
40. Yang, B., Zhang, X. & Zhao, M. Dirac node lines in two-dimensional Lieb lattices. *Nanoscale* **9**, 8740–8746 (2017).
41. Shirer, K. R. et al. Dirac fermions in the heavy-fermion superconductors Ce(Co,Rh,Ir)In_5. https://arxiv.org/abs/1808.00403 (2018).
42. Denlinger, J. D. et al. SmB 6 photoemission: past and present. in *Proceedings of the International Conference on Strongly Correlated Electron Systems (SCES2013)* (Journal of the Physical Society of Japan, 2014).
43. Korotin, Dm. M. et al. Magnetic ordering in intermetallic $La_{1-x}Tb_xMn_2Si_2$ compounds. *J. Magn. Magn. Mater.* **454**, 144–149 (2018).
44. Korotin, Dm. M. et al. Origin of magnetic phase transition in RMn_2Si_2 (R = rare-earth ion or Y) intermetallics. *Comput. Mater. Sci.* **184**, 109901 (2020).
45. Strocov, V. N. et al. Soft-X-ray ARPES facility at the ADRESS beamline of the SLS: concepts, technical realisation and scientific applications. *J. Synchrotron Rad.* **21**, 32–44 (2014).
46. Strocov, V. N. et al. High-resolution soft X-ray beamline ADRESS at the Swiss Light Source for resonant inelastic X-ray scattering and angle-resolved photoelectron spectroscopies. *J. Synchrotron Rad.* **17**, 631–643 (2010).
47. Strocov, V. N. Intrinsic accuracy in 3-dimensional photoemission band mapping. *J. Electron Spectrosc. Relat. Phenom.* **130**, 65–78 (2003).
48. Strocov, V. N. et al. Three-dimensional electron realm in VSe_2 by soft-X-ray photoelectron spectroscopy: origin of charge-density waves. *Phys. Rev. Lett.* **109**, 086401 (2012).
49. Giannozzi, P. et al. QUANTUM ESPRESSO: a modular and open-source software project for quantum simulations of materials. *J. Phys.: Condens. Matter* **21**, 395502 (2009).
50. Giannozzi, P. et al. Advanced capabilities for materials modelling with quantum ESPRESSO. *J. Phys.: Condens. Matter* **29**, 465901 (2017).
51. Giannozzi, P. et al. Quantum ESPRESSO toward the exascale. *J. Chem. Phys.* **152**, 154105 (2020).
52. Perdew, J. P. et al. Restoring the density-gradient expansion for exchange in solids and surfaces. *Phys. Rev. Lett.* **100**, 136406 (2008).
53. Prandini, G., Marrazzo, A., Castelli, I. E., Mounet, N. & Marzari, N. Precision and efficiency in solid-state pseudopotential calculations. *npj Comput Mater.* **4**, 1–13 (2018).
54. Kalychak, Ya. M. et al. Crystalline structures of compounds $RCoin_5$ (R = Ce, Pr, Nd, Sm, Gd, Tb, Dy, Ho, Y) and R_2Coln_8 (R = Ce, Pr, Nd, Sm, Gd, Dy, Ho, Er, Tm, Y). *Russian Metallurgy* **1**, 213–215 (1989).
55. Zagorac, D., Müller, H., Ruehl, S., Zagorac, J. & Rehme, S. *J. Appl. Cryst*. **52**, 918–925. https://doi.org/10.1107/S160057671900997X (2019).
56. Cococcioni, M. & de Gironcoli, S. Linear response approach to the calculation of the effective interaction parameters in the LDA + U method. *Phys. Rev. B* **71**, 035105 (2005).
57. Timrov, I., Marzari, N. & Cococcioni, M. Hubbard parameters from density-functional perturbation theory. *Phys. Rev. B* **98**, 085127 (2018).
58. Timrov, I., Marzari, N. & Cococcioni, M. HP—a code for the calculation of Hubbard parameters using density-functional perturbation theory. *Comput. Phys. Commun.* **279**, 108455 (2022).
59. Pacilè, D. et al. Narrowing of d bands of FeCo layers intercalated under graphene. *Appl. Phys. Lett.* **118**, 121602 (2021).
60. Tam, D. W. et al. Flat-band hybridization between f and d states near the Fermi energy of $SmCoIn_5$. Materials Cloud Archive, https://doi.org/10.24435/materialscloud:zc-45 (2023).

Acknowledgements

This research was supported by the Swiss National Science Foundation (SNSF) under grant 200021_184983 (M.K.), and by the NCCR MARVEL, a National Centre of Competence in Research, funded by the Swiss National Science Foundation (grant number 205602) (N.C.). D.W.T. acknowledges funding from the European Union's Horizon 2020 research and innovation program under the Marie Skłodowska-Curie grant agreement No. 884104 (PSI-FELLOW-III-3i). F.A. acknowledges support by Swiss National Science Foundation Project No. 206312019002.

Author contributions

D.W.T. and M.K. conceived the work and guided the project. D.J.G. and E.P. prepared samples, D.W.T. and F.A. prepared and conducted ARPES experiments with guidance from V.N.S., and N.C. performed density functional theory calculations. D.W.T., M.K., and N.C. prepared the manuscript with input from all authors.

Competing interests

The authors declare no competing interests.

Additional information

Supplementary information The online version contains supplementary material available at https://doi.org/10.1038/s41535-024-00632-8.

Correspondence and requests for materials should be addressed to David W. Tam or Michel Kenzelmann.